International Journal of Machining and Machinability of Materials

ISSN online: 1748-572X - ISSN print: 1748-5711
https://www.inderscience.com/ijmmm

Optimising the parameters in AWJT process using a modified multi-objective DE algorithm

I.R. Gawai, D.I. Lalwani

DOI: 10.1504/IJMMM.2025.10068694

Article History:

Received:	26 August 2023
Last revised:	02 December 2023
Accepted:	29 December 2023
Published online:	18 March 2025

Optimising the parameters in AWJT process using a modified multi-objective DE algorithm

I.R. Gawai* and D.I. Lalwani

Department of Mechanical Engineering,
Sardar Vallabhbhai National Institute of Technology,
Ichchhanath Circle, Athawa Lines, Surat, Gujarat, 395007, India
Email: gawai.ishan@gmail.com
Email: dil@med.svnit.ac.in
*Corresponding author

Abstract: This paper presents a novel multi-objective optimisation algorithm for predicting the optimal control parameters of a radial abrasive water jet turning (AWJT) method. The objective is to maximise the material removal rate (MRR) and minimise the surface roughness (R_a) of the turned surface. The control parameters include water pressure, jet feed speed, abrasive flow rate, surface speed, and nozzle tilted angle. The proposed algorithm, called multi-objective amended differential evolution algorithm (MADEA), is a rank-based differential evolution (DE) algorithm that uses non-dominated sorting and crowding distance to select and update the solutions. The performance of MADEA is compared with six state-of-the-art multi-objective evolutionary algorithms on a set of benchmark test problems and the AWJT problem. The results show that MADEA can find better Pareto optimal solutions than the other algorithms.

Keywords: multi-objective optimisation; ADEA; AWJT; turning; efficient non-dominated sorting; ENS; evolutionary algorithms.

Reference to this paper should be made as follows: Gawai, I.R. and Lalwani, D.I. (2025) 'Optimising the parameters in AWJT process using a modified multi-objective DE algorithm', *Int. J. Machining and Machinability of Materials*, Vol. 27, No. 1, pp.19–39.

Biographical notes: I.R. Gawai is a research scholar at Sardar Vallabhbhai National Institute of Technology, Surat, India. His expertise is in evolutionary optimisation, metaheuristics and design engineering.

D.I. Lalwani is an Associate Professor at Sardar Vallabhbhai National Institute of Technology, Surat, India. His areas of expertise are evolutionary optimisation, design engineering, non-conventional machining processes, conventional machining processes and dynamics of vibrations.

1 Introduction

Abrasive water jet machining (AWJM) is a hybrid process that combines abrasive jet machining (AJM) and water jet machining (WJM). In this process, a high-speed water jet containing abrasives erodes the material through impact and abrasion. AWJM can

perform various operations, such as cutting, drilling and turning, on different materials, such as metals, alloys, glass, composites and acrylics (Arun et al., 2023; Balasubramaniyan et al., 2023). The benefits of AWJM include omnidirectional cutting capability, minimal thermal effects, burr-free edges and high efficiency. Figure 1 illustrates the working principle of AWJM. A high-velocity water jet adhering abrasive particle is targeted towards the workpiece. The high momentum of the water jet gets transferred to the abrasives and as a result, a large quantity of abrasive particles accelerates. The accelerated abrasives impinge on the workpiece and erode it.

Figure 1 Abrasive water jet machining

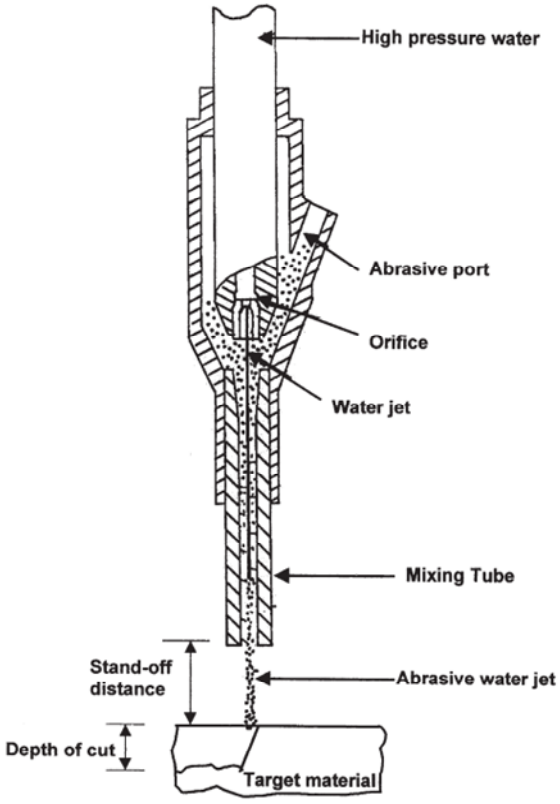

Source: Jain et al. (2001)

The abrasive water jet turning (AWJT) is based on abrasive water jet cutting. Similar to conventional turning, the workpiece is rotated at cutting axis, and the jet is traversed to remove material and obtain an axisymmetric shape. Figure 2 shows the turning modes of the AWJT. Figure 2(a) shows the offset mode, and Figure 2(b) shows the radial mode of AWJT. In radial mode, the position of the nozzle is directly above the axis of the workpiece, whereas in offset turning, the nozzle is situated at the periphery of the workpiece. The AWJT shows consistent advantages when handling various types of materials. Flögel and Faltin (2013) turned titanium alloy, Ti6A14V, with AWJT. The effects on tool life in terms of volume, material removal rate (*MRR*) and surface roughness (R_a) caused due to five parameters of AWJT, adjusted depth of cut (d), feed

(F), speed (n), particle size (d_p), and abrasive flow rate (m_A), were studied. The authors suggested that AWJT can be used as an economical alternative manufacturing process for rough turning of titanium alloys. Yue et al. (2013) conducted an experimental study of the radial-mode AWJT of 96% alumina ceramics. The process parameters n, F, m_A, water pressure (P_W), and nozzle tilted angle (β) were explored to study the effects on depth of turning, i.e., d and *MRR*. The parameters' effectiveness was studied using range analysis and variance analysis, in which authors found that the feed speed affects the depth of turning the most. Yue et al. (2014a) extended their study by using response surface methodology (RSM) and sequential approximation optimisation (SAO), to explore the effects of AWJT parameters on *MRR*. Yue et al. (2014a) also gave mathematical models for *MRR* and R_a. In the current study, the same models were optimised and compared with other multi-objective algorithms. Yue et al. (2014a) concluded that water pressure and abrasive mass flow rate has a high effect on *MRR*. Liu et al. (2013) studied the effect of standoff distance (*SOD*) on depth of penetration or d, R_a, and actual impact angle or β. The study was carried out on both modes of AWJT of alumina (Al_2O_3) ceramics, where authors found that *SOD* plays a significant role in radial-mode AWJT and has almost no effect in offset-mode AWJT. Zohourkari et al. (2015) carried out AWJT operation on AA2011-T4 alloy. A design model of five AWJT parameters was created using a five-level central composite rotatable experimental design. Using the analysis of variance (ANOVA) approach, a polynomial model for *MRR* was created, and the significance of each parameter was tested. Uhlmann et al. (2014) used AWJT for the rough turning of G-$AlSi_{17}Cu_4Mg$ alloy. The final pass was done using a conventional turning process. By combining both turning processes, a high product yield can be obtained, as the tool life of AWJT was at least ten hours at *MRR* of 13 cm^3/min. Also, negligible thermal stresses were exerted during rough passes. As a result, a high surface finish was achieved by the combination of AWJT roughing and conventional finishing. Two ceramics, 96% alumina and 95% zirconia, were turned in radial mode using AWJT and studied by Yue et al. (2014b). The material removal mechanism of both ceramics was studied on microscopic level. It was seen that 96% alumina showed brittle fracture caused by intergranular cracks and fragmentations, whereas 95% zirconia showed plastic deformation with some pits. AWJT process can also be used for non-metals. Kartal et al. (2014) investigated the average surface roughness and *MRR* obtained for AWJT of low density polyethylene (LDPE). The process parameters of AWJT were manipulated in order to get optimum surface quality and MRR. The experiments were conducted according to the Taguchi L27 orthogonal full factorial design and optimisation box and ANOVA were used for analysis of the results. Kartal and Gökkaya (2015) observed the most significant parameter in AWJT of AISI 1050 steel material. Kartal and Gökkaya (2015) considered sets of five parameters, F, m_A, lathe spin rate (n), nozzle distance or *SOD*, and nozzle diameter (d_N); they observed that F had the highest impact on R_a, and m_A had a significant effect on MRR. Kartal and Yerlikaya (2016) extended their research on AWJT of non-metals, from LDPE to polytetrafluoroethylene (PTFE), castamide, and polyamide (PA). This time, three process parameters, F, m_A, and n, were considered for optimisation. The three process parameters were changed according to predefined sets of values to obtain optimum average R_a and *MRR*. It was observed that the objectives, average R_a and *MRR*, were highly affected by the F. Kartal et al. (2017) also optimised the AWJT of Al-6082 T6 alloy by manipulating four process parameters, F, m_A, n and *SOD*. They found that the best surface finish was obtained at higher n and m_A, and lower F and *SOD*. Ibrahim et al. (2020) conducted AWJT process on a submerged castamide workpiece. Three input

variables or process parameters were considered for getting minimum R_a and maximum *MRR*. The input variables were nozzle traverse speed or *F*, *mA* and *n*. It was found that by submerging the workpiece, the surface roughness increased and *MRR* decreased. The effect of parameters was studied using ANOVA, and the optimisation was carried out using TOPSIS and VIKOR methods. Kartal and Kaptan (2023) investigated the AWJT of acrylonitrile butadiene styrene (ABS) and polylactic acid (PLA). The parameters considered were nozzle feed, abrasive flow rate, chuck turning speed and nozzle distance. They concluded that by increasing the rotational speed, the surface roughness decreased. Štefek et al. (2021) investigated the effect of AWJT parameters in tangential or offset-mode turning. The three parameters considered were, traverse speed, i.e., *F*, rotational speed, i.e., *n*, and relative position of the jet, i.e., *SOD*. The authors stated that the *SOD* was the key parameter to achieve highest efficiency. Kasim et al. (2022) studied the effects of parameters in AWJT of Inconel 718 for obtaining minimum surface roughness. The experiments were carried out according to the two-level full factorial design for three process parameters, *d*, *F*, and *n*. The values of input and output, R_a, were correlated using design of experiments (*DOE*) method and the significance of the parameters was calculated using ANOVA method. The key parameter for good surface finish was *d*.

Figure 2 AWJT modes

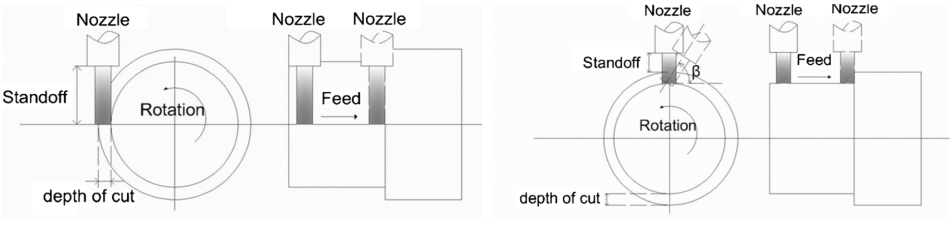

(a) (b)

Source: Yue et al. (2014a)

In the current study, the AWJT of alumina ceramic (Yue et al., 2014a) is optimised using evolutionary algorithms. As per the authors' observation, the AWJT process has never been optimised using evolutionary algorithms. Most optimisations were carried out using statistical methods like the *DOE* or the TOPSIS method. However, the aim of the current study is to introduce the capability of multi-objective amended differential evolution algorithm (MADEA) in solving real-life problems. It will be interesting to compare the optimum values of parameters obtained using conventional methods and multi-objective evolutionary algorithms.

The rest of the paper is organised as follows. Section 2 introduces multi-objective optimisation problem (MOP) and the AWJT problem. Also, the variant of the differential evolution (DE) algorithm is explained using pseudo code in the same section. In Section 3, the multi-objective amended differential evolution algorithm (MADEA) is described. The results are shown in Section 4 and the paper is concluded in Section 5.

2 Preliminary information

2.1 Multi-objective optimisation problem

The general form of MOOP is given in equation (1).

$$\begin{aligned} &\text{Maximise/minimise} \quad f_m(x) \quad m = 1, 2, ..., M \\ &\text{Subject to} \qquad\quad g_j(X) \geq 0 \quad j = 1, 2, ..., J \\ &\qquad\qquad\quad h_k(X) = 0 \quad k = 1, 2, ..., K \\ &\qquad\qquad\quad X_i^{(L)} \leq X_i \leq X_i^{(U)} i = 1, 2, ..., n \end{aligned} \tag{1}$$

where M is the number of objectives, J is the number of inequality constraints, and K is the number of equality constraints. $X_i^{(U)}$ and $X_i^{(L)}$ are the variable bounds which together form a decision variable space or decision space. The individual in the population is also called a vector, and the individual on which the operations are conducted is known as a current or target individual/vector.

The problem considered in this paper is adopted from Yue et al. (2014a), and it has two objectives and no constraints. The adopted model of the AWJT method is given in equations (2) and (3).

Maximise, *MRR*

$$\begin{aligned} Y_1 = {} & 3814.35 + 943.50X_1 - 530.29X_2 + 745.01X_3 + 154.82X_4 - 193.65X_5 \\ & + 551.62X_1X_3 + 284.87X_1X_5 - 147.61X_2X_5 - 225.72X_3X_4 + 345.29X_2^2 \\ & - 483.49X_3^2 - 430.00X_4^2 \end{aligned} \tag{2}$$

Minimise, R_a

$$\begin{aligned} Y_2 = {} & 3.78 + 0.31X_1 + 0.04X_2 - 0.38X_3 + 0.087X_4 + 0.046X_5 - 0.24X_1X_2 \\ & - 0.067X_4X_5 - 0.17X_2^2 + 0.17X_3^2 + 0.14X_5^2 \end{aligned} \tag{3}$$

where X_1 is water pressure (P_w, MPa), X_2 is jet feed speed (F, mm/s), X_3 is abrasive mass flow rate (m_A, g/s), X_4 is surface speed (n, m/s), and X_5 is the nozzle tilted angle ($\beta°$). The parameter bounds are as follows. $190 \leq X_1 \leq 310$, $0.05\ X_2 \leq 0.25$, $3.5 \leq X_3 \leq 11.5$, $1.5 \leq X_4 \leq 9.5$, $45 \leq X_5 \leq 105$. Both objectives conflict with each other. With higher MRR, the surface roughness, R_a, increases. Therefore, a set of trade-off solutions or a Pareto solution set can help the decision maker to choose a set of parameters according to their needs.

2.2 Amended differential evolution algorithm

The DE algorithm is applicable to unconstrained optimisation problems. Rana and Lalwani (2017) introduced a few amendments to DE algorithm to solve constrained single-objective optimisation problems. The modified DE algorithm is called an amended differential evolution algorithm (ADEA). In addition to convert DE into a constrained optimisation algorithm, a few amendments were added to increase DE's performance. The ADEA have shown competitive results, and some reported solutions were even better than the benchmark problems from CEC 2006 (Runarsson et al., 2006). The first amendment is to utilise a random population produced using the design of experiment

approach (RPDoE). The pseudocode of RPDoE is given in Algorithm 1. The use of RPDoE results in better coverage of the search space, which results in better exploration and hence, better results.

Algorithm 1 RPDoE

Input: LB, UB, n

Output: Initial population of size [(2^D + 2xD + 1) x n]-by-¬D

1 Create x = []

2 Using $\boldsymbol{x_{mb1}} = \boldsymbol{X_{j,i}^{(L)}} + \left(\frac{\boldsymbol{X_{j,i}^{(U)}} - \boldsymbol{X_{j,i}^{(L)}}}{3}\right)$ and $\boldsymbol{x_{mb2}} = \boldsymbol{X_{j,i}^{(L)}} + 2\times\left(\frac{\boldsymbol{X_{j,i}^{(U)}} - \boldsymbol{X_{j,i}^{(L)}}}{3}\right)$, divide the variable bounds into levels –1, 0 and 1.

3 Use divided bounds to create (2^D + 2xD + 1) subspaces.

4 Generate n number of random individuals in each subspace.

5 Merge x and random individuals created in subspaces

6 return x

The DE is sensitive to the parameters and often a better individual may get thrown off to a worse place in the mutation process. Takahama and Sakai (2009) came up with the idea of having a range of parameters and ranking. In the second amendment, the individuals are ranked according to the objective value and each individual is assigned the scaling factor and crossover probability value according to their respective rank. Individuals with higher rankings will be given a lower scaling factor and a higher crossover probability, ensuring that the respective individuals are perturbed less, and the elements in that individual are always chosen in the crossover process. Better exploration of search space results in a better optimum solution. In DE, the exploration is brought by the mutation process. In ADEA, two mutant individuals are created instead of one. Among the 2NP mutant individuals, top NP individuals are selected and proceed towards the crossover process. The complete procedure of ADEA is given in Algorithm 2.

Algorithm 2 ADEA

1 Values of F_{min}, F_{max} and Cr_{min}, Cr_{max} are assumed.

2 The initial population, X_i, is generated using RPDoE and the objective function ($\boldsymbol{f}$) is calculated for each individual, $\boldsymbol{f}(X_i)$

3 Sort $\boldsymbol{f}(X_i)$ and choose top NP individuals

4 Rank individuals, $\boldsymbol{R_i}$

5 Calculate the values of F and Cr for each member according to the equation
$\boldsymbol{F_{i,g}} = \boldsymbol{F_{min}} + (\boldsymbol{F_{max}} - \boldsymbol{F_{min}})\left(\frac{\boldsymbol{R_i} - 1}{\boldsymbol{NP} - 1}\right)$ and $\boldsymbol{Cr_{i,g}} = \boldsymbol{CR_{max}} - (\boldsymbol{CR_{max}} - \boldsymbol{CR_{min}})\left(\frac{\boldsymbol{R_i} - 1}{\boldsymbol{NP} - 1}\right)$

6 while Stopping criteria is False do

7 for i = 1:NP do

8 Choose random individuals x_{r1}, x_{r2} and x_{r3}, s.t., r1 ≠ r2 ≠ r3 ≠ i

9 Create two mutant individuals, $\mathfrak{m}_1$ and $\mathfrak{m}_2$, using the equation $\mathfrak{m}\mathbf{1_i} = \boldsymbol{X_{r_1}} + \boldsymbol{F_i}(\boldsymbol{X_{r_2}} - \boldsymbol{X_{r_3}})$ and $\mathfrak{m}\mathbf{2_i} = \boldsymbol{X_{r_1}} - \boldsymbol{F_i}(\boldsymbol{X_{r_2}} - \boldsymbol{X_{r_3}})$

Select top NP individuals from 2NP mutant individuals and form mutant individual $\mathfrak{m}_i$
for j = 1:D do
Choose jrand, a random integer between 1 to D
Choose μ, a random number between 0 to 1.
Calculate trial vector,

$$\mathbf{U}_{j,i} = \begin{cases} \mathfrak{m}_{j,i} & \text{if } (\boldsymbol{\mu} \le \boldsymbol{Cr} \textbf{ or } \boldsymbol{j} = \boldsymbol{j}_{rand}) \\ \mathbf{X}_{j,i} & \end{cases}$$

end for
Compute combined function for trial vector, $\boldsymbol{f}(U_i)$
if ($\boldsymbol{f}(U_i)$ is nearer to optimum point than $\boldsymbol{f}(X_i)$) do
$X_i = U_i$
end if
end for
end while
Solution: X_i

3 Methodology

3.1 Multi-objective amended differential evolution algorithm

This section of the paper explains the formulation of MADEA. The ADEA algorithms is incorporated with an archive approach, an efficient non-dominated sorting (ENS) method (Zhang et al., 2015) and a crowding distance (CD) process (Deb et al., 2002) to solve MOPs. The ENS method bifurcates the given population into number of fronts, and the CD process is used to sort and rank the individuals. The CD process also retains the diversity in the solution, as it scores an individual based on its distance from the neighbouring individuals. Equation (3) is used to calculate the CD.

$$CD_{I_j^m} = CD_{I_j^m} + \frac{f_m^{\left(I_j^m+1\right)} - f_m^{\left(I_j^m-1\right)}}{f_m^{\max} - f_m^{\min}} \tag{3}$$

where $f_m^{\max}$ and $f_m^{\min}$ are the maximum and minimum values of m^{th} objective function. I_j is the solution index of j^{th} member in descending list of m^{th} objective function.

Figure 3 shows the flowchart of MADEA. The complete procedure to apply MADEA on a MOP is given in Algorithm 4.

3.2 ENS algorithm

In the ENS approach, the duplicate comparisons are eliminated, which makes the algorithm very efficient and faster. The detailed working of ENS is given in Algorithm 3. There are two conditions which $Fr[k]$ has to satisfy to get solution s_n assigned to it:

1 At least one solution from front $Fr[j]$ that has been assigned should dominate solution s_n, where $1 \le j \le k - 1$.

2 No solutions from front $Fr[l]$ should dominate solution s_n, where $l \geq k$.

Figure 3 MADEA flowchart (see online version for colours)

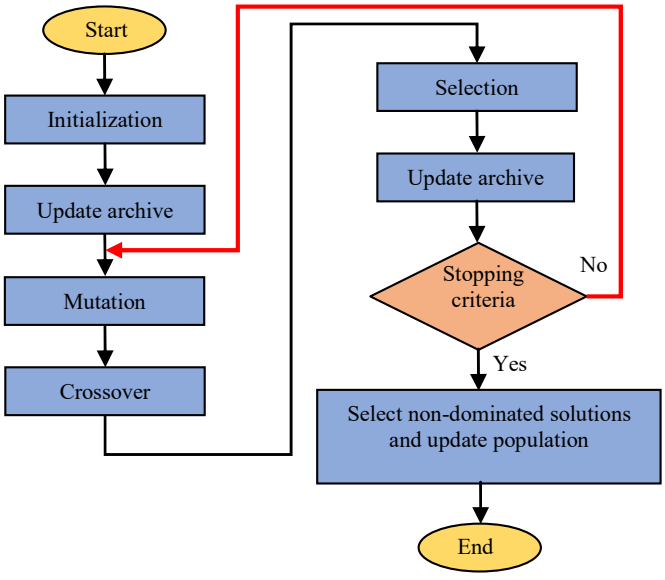

Figure 4 illustrates how the ENS conditions need to be satisfied to assign solution s_n to a particular front. In the proposed algorithm, a sequential search (SS) strategy is adopted.

Algorithm 3 ENS

Input: Solution set

Output: The set of fronts

```
Set of fronts, Fr = []
Sort solution set, S, by the first objective's value
for s = sorted S do
NF = sizeof(Fr), i.e., number of fronts discovered
k = 1
while true do
    compare solutions in Fr[k] from last to first with si where, i = 1:sizeof(S)
    if solutions in Fr[k] do not dominate si
        add si to Fr[k]
        return k
        break
    else
        k = k + 1
        if k > s
            create new front and add si to it
            return NF + 1
```

```
            break
        end if
    end if
end while
end for
return Fr
```

Figure 4 Assignment process of solutions s_n to a front, using ENS method (see online version for colours)

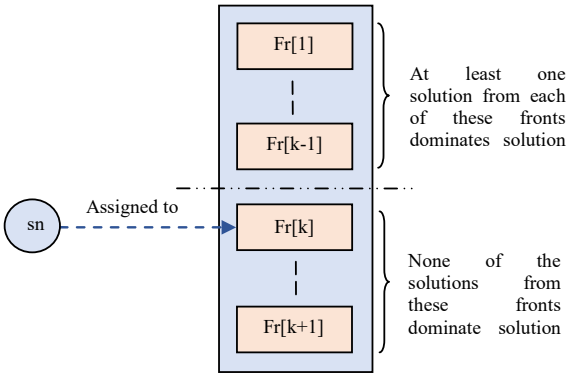

Algorithm 4 MADEA

1 Values of F_{min}, F_{max} and Cr_{min}, Cr_{max} are initialised.
2 The Archive is set to *null*
3 The initial population, X_i, is generated using OBL and combined functions are calculated for each individual, $\boldsymbol{f}(X_i)$
4 Determine the fronts in the initial population using ENS
5 Add non-dominated solutions in the archive and eliminate dominated solutions from the archive
6 Sort $\boldsymbol{f}(X_i)$ using crowding distance and choose the top NP individuals
7 while Stopping criteria is False do
8 Rank individuals
9 Calculate the values of F and Cr for each member according to the equation

$$\boldsymbol{F}_{i,g} = \boldsymbol{F}_{min} + (\boldsymbol{F}_{max} - \boldsymbol{F}_{min})\left(\frac{\boldsymbol{R}_i - 1}{\boldsymbol{NP} - 1}\right) \text{ and } \boldsymbol{Cr}_{i,g} = \boldsymbol{CR}_{max} - (\boldsymbol{CR}_{max} - \boldsymbol{CR}_{min})\left(\frac{\boldsymbol{R}_i - 1}{\boldsymbol{NP} - 1}\right)$$

10 for i = 1:NP do
11 Choose random individuals x_{r1}, x_{r2} and x_{r3}, s.t., r1 ≠ r2 ≠ r3 ≠ i
12 Create two mutant individuals, $\mathfrak{y}\mathbf{1}_i = \boldsymbol{X}_{r_1} + \boldsymbol{F}_i(\boldsymbol{X}_{r_2} - \boldsymbol{X}_{r_3})$ and $\mathfrak{y}\mathbf{2}_i = \boldsymbol{X}_{r_1} - \boldsymbol{F}_i(\boldsymbol{X}_{r_2} - \boldsymbol{X}_{r_3})$
13 end for
14 Merge mutant population, $\mathfrak{y}_1$ and $\mathfrak{y}_2$, to form $\mathfrak{z}$ of size 2NP
15 For each mutant individual, find the front and sort $\boldsymbol{f}(\mathfrak{z}_i)$ according to crowding distance.

Add non-dominated solutions in the archive and eliminate dominated solutions from the archive
Select top NP individuals from 2NP mutant individuals
for i = 1:NP do
  for j = 1:D do
    Choose jrand, a random integer between 1 to D
    Choose μ, a random number between 0 to 1.
    Calculate trial vector,
    $$\mathbf{U}_{j,i} = \begin{cases} \mathfrak{m}_{j,i} & \text{if } (\boldsymbol{\mu} \le \boldsymbol{Cr} \textbf{ or } \boldsymbol{j = j_{rand}}) \\ \mathbf{X}_{j,i} & \end{cases}$$
  end for
end for
Compute objective functions for trial vector, $\boldsymbol{f}(U_i)$
Merge U_i and X_i to form Ʃ
Sort $\boldsymbol{f}$(Ʃ) using ENS and CD process to choose top NP individual from Ʃ
Add non-dominated solutions in the archive and eliminate dominated solutions from the archive
end while
Solution: The archive

4 Results and discussion

The MADEA algorithm is validated by comparing the inverted generational distance (IGD) values of 15 benchmark functions from CEC 2017 with five different multi-objective optimisation evolutionary algorithms (MOEAs), namely MWDEO, MaOEA CS, NSGA III, A-NSGA III and GrEA (Ewees et al., 2021). The MADEA algorithm parameters are set as follows:

Minimum scaling factor, F_{min}	0.5
Maximum scaling factor, F_{max}	0.8
Minimum crossover probability, Cr_{min}	0.8
Maximum crossover probability, Cr_{max}	0.9
Population size, *NP*	200
Archive size, 2*NP*	400
Number of generations, *maxgen*	2,000
Number of trials	30

The $\overline{f}$ is the best mean IGD value, std is standard deviation and rank is position of algorithm.

Table 1 reveals that MADEA obtained better answers for 9 out of 15 benchmark problems. This supports the use of MADEA for the optimisation of parameters of AWJT.

Table 1 IGD values of benchmark functions from CEC 2017 obtained using MADEA

		MWDEO	*MaOEA CS*	*NSGA III*	*A-NSGA III*	*GrEA*	*MADEA*
1	$\overline{f}$	0.0312	0.0425	0.0611	0.0459	0.0411	0.0345
	std	0.0015	0.0025	0.0014	0.0008	0.001	0.0016
	Rank	1	4	6	5	3	2
2	$\overline{f}$	0.0157	0.0349	0.0368	0.0326	0.0318	0.0283
	std	0.0005	0.0035	0.0005	0.001	0.0007	0.0011
	Rank	1	5	6	4	3	2
3	$\overline{f}$	191.09	119.94	253.88	323.22	152.64	110.1743
	std	200.41	206	213	273	173	172.7205
	Rank	4	2	5	6	3	1
4	$\overline{f}$	23.857	24.735	34.986	35.905	27.378	69.4877
	std	2.533	14.9	18.9	15.9	9.82	62.8969
	Rank	1	2	4	5	3	6
5	$\overline{f}$	0.35	0.3668	0.5033	0.5402	0.6006	0.1870
	std	0.3147	0.388	0.56	0.59	0.565	0.0062
	Rank	2	3	4	5	6	1
6	$\overline{f}$	0.0194	0.0179	0.0132	0.0109	0.0167	0.0014
	std	0.0021	0.0077	0.0019	0.001	0.001	4.91E-05
	Rank	6	5	3	2	4	1
7	$\overline{f}$	0.1196	0.1271	0.0998	0.1002	0.0796	0.1367
	std	0.0779	0.0355	0.0112	0.0113	0.0035	0.0227
	Rank	4	5	2	3	1	6
8	$\overline{f}$	0.164	0.1773	0.7907	0.4557	0.3502	0.0391
	std	0.0923	0.0378	0.537	0.372	0.261	0.0006
	Rank	2	3	6	5	4	1
9	$\overline{f}$	0.3392	0.2398	0.4092	0.3156	0.473	0.0547
	std	0.5782	0.045	0.524	0.232	0.23	0.0359
	Rank	4	2	5	3	6	1
10	$\overline{f}$	1.1487	1.6706	1.1362	1.1112	0.8975	1.1485
	std	0.4878	0.138	0.0966	0.0867	0.0721	0.1709
	Rank	5	6	3	2	1	4
11	$\overline{f}$	0.2224	0.2797	0.196	0.2358	0.2474	0.1071
	std	0.0144	0.0477	0.0242	0.0439	0.0344	0.0024
	Rank	3	6	2	4	5	1

Table 1 IGD values of benchmark functions from CEC 2017 obtained using MADEA (continued)

		MWDEO	*MaOEA CS*	*NSGA III*	*A-NSGA III*	*GrEA*	*MADEA*
12	$\overline{f}$	0.1628	0.3347	0.2457	0.2582	0.2396	0.1551
	std	0.0117	0.078	0.023	0.0103	0.0065	0.0024
	Rank	2	6	4	5	3	1
13	$\overline{f}$	0.132	0.124	0.1021	0.1048	0.1642	0.0691
	std	0.0274	0.0193	0.0125	0.0142	0.0249	0.0160
	Rank	5	4	2	3	6	1
14	$\overline{f}$	3.9052	3.921	4.0185	3.9163	3.9344	10.8126
	std	0.7527	1.49	0.896	0.778	0.967	1.7793
	Rank	1	3	5	2	4	6
15	$\overline{f}$	0.5842	0.6494	1.7378	1.6416	0.8314	0.2536
	std	0.284	0.235	0.318	0.277	0.133	0.0294
	Rank	2	3	6	5	4	1

The parameters for the AWJT problem are set as follows:

Minimum scaling factor, $F_{\min}$	0.5
Maximum scaling factor, $F_{\max}$	0.8
Minimum crossover probability, $Cr_{\min}$	0.8
Maximum crossover probability, $Cr_{\max}$	0.9
Population size, *NP*	100
Archive size, 2*NP*	200
Number of generations, *maxgen*	1,000
Number of trials	30

Figure 5 shows the Pareto fronts calculated by all seven algorithms and the true Pareto front. The enlarged image of Pareto fronts shown in Figure 6 represents that the MADEA was able to surpass the true Pareto front. The Pareto front obtained by MADEA performs better than the true Pareto front in 149 instances. This means that the 149 solutions found by MADEA dominate the solutions in the true Pareto front. All 149 solutions are provided in Appendix of the paper. Also, the true Pareto front is a set of non-dominated solutions calculated using six competing algorithms. The star marker in Figure 5 represents the solution reported by Yue et al. (2014a). It can be seen that the solutions found using evolutionary algorithms have dominated the solution obtained using statistical methods.

The performance metrics are calculated for all the competing algorithms, NSGA II, NSGA III, MOEA/D, MOPSO, PESA2 and SPEA2, and for the archive of the best trial of MADEA. The comparison of the results is shown in Table 2. The performance metrics used for comparison are the IGD (Coello and Cortés, 2005), spacing (Schott, 1995), coverage (Zitzler and Thiele, 1999), coverage over Pareto front (CPF) (Tian et al., 2019), average Hausdorff distance or ΔP (Schutze et al., 2012), metric for diversity (DM) (Deb

and Jain, 2002) and pure diversity (PD) (Wang et al., 2017). The best values are represented in bold letters in Table 2.

The performance metrics analyse the convergence, diversity and uniformity of the Pareto front. The IGD metric and ΔP can be held accountable for convergence and diversity (Wang et al., 2017). It can also be seen from Table 2 that the values of IGD and ΔP are identical. However, the ΔP calculates the average distance between the image of the obtained Pareto set and the considered true Pareto front. The solution with lower value IGD, and commutatively ΔP, is considered as a good-quality solution. The comparison shows NSGA II has performed well in terms of IGD and ΔP metrics. But, as seen in Figure 5, the Pareto front of MADEA surpasses the considered true Pareto front. For distance-based metrics, the value is based on the distance between the solutions; it does not matter if the solution dominates the considered true Pareto solution. Hence, the value of IGD and ΔP metrics should not be considered for determining the performance of MADEA.

Figure 5 Pareto fronts of AWJM (see online version for colours)

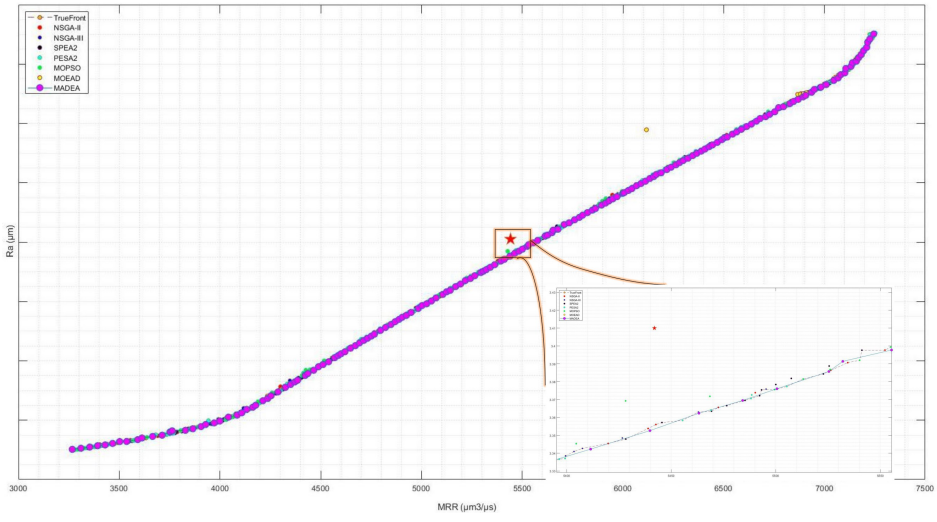

Diversity with evenly spread individuals over the true Pareto curve is always desired. The spacing value is equal to zero when all the solutions are equally spaced from each other. One can see from Figure 5 that the solutions in the Pareto front of MADEA are not uniformly spaced. Therefore, in terms of spacing the MADEA ranks fourth among the competition. The PD metric gives a high value to evenly spread solution over the true Pareto front. PD values show the number of non-matching solutions spread across the true Pareto front or curve. As MADEA has solutions better than the true Pareto front, the PD value for MADEA is not the highest. The metric for diversity (DM), encourages the algorithm to diversify the solutions. Hence, a higher value of DM represents a more diverse solution. MADEA achieved the highest value of DM, which shows that it managed to obtain a very diverse solution, but lower values of spacing and PD represent its inability to obtain a uniformly spread Pareto front.

The value of coverage ranges from [0, 1]. It is an indicator of a number of solutions in the true Pareto sets dominated by the obtained Pareto solutions. Coverage equals 1 represents that all the solutions are dominated by the true Pareto front. In contrast , if

coverage is equal to zero, then the considered true Pareto front is dominated by the obtained solutions. Here, the considered true Pareto front is made up of all non-dominated solutions from six algorithms. Hence, their Pareto front is dominated by the considered true Pareto front, whereas the value 0.395 for MADEA shows that the Pareto front of MADEA has dominated the considered true Pareto front. The CPF or the coverage over Pareto front is an indicator which tells the volume of obtained front covers the volume of true Pareto front. Therefore, the higher value of CPF represents that the obtained solutions are lying over the true Pareto front. Here, the MADEA has a better Pareto front than the considered true Pareto front. Hence, the algorithm with maximum number of solutions in the considered true Pareto front would have a high CPF value. As NSGA-II contributes maximum non-dominated solutions in the considered true Pareto front, its CPF is the highest.

Figure 6 Enlarged image of Pareto fronts (see online version for colours)

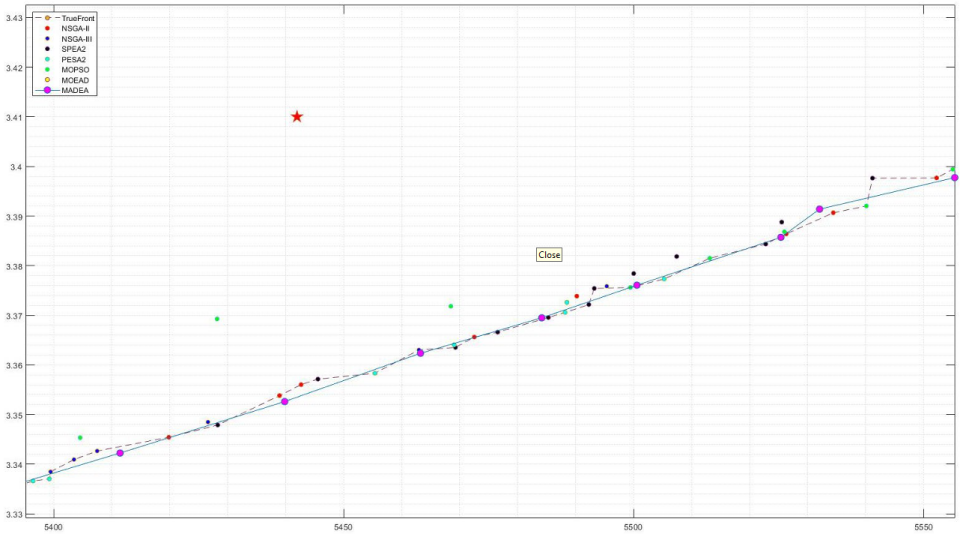

Table 2 Comparison of MADEA using performance metrics

	IGD	*Spacing*	*Coverage*	*CPF*	*ΔP*	*DM*	*PD*
NSGA II	*5.379706*	7.852304	1	*0.812254*	*5.379706*	0.82571	*411,872.7*
NSGA III	17.56771	12.48609	1	0.515169	17.56771	0.667419	218,277.1
MOEA/D	936.0047	0.979951	1	0.000746	936.0047	0.031228	26,259.86
MOPSO	7.450604	10.39444	1	0.68572	7.450604	0.762383	321,881.7
PESA2	8.575072	10.95839	1	0.583758	8.575072	0.696595	231,266.8
SPEA2	6.775378	8.04123	1	0.770266	6.775378	0.742949	284,719.6
MADEA	6.267091	10.0254	*0.395*	0.656261	6.267091	*0.82853*	271,305.7

5 Conclusions

In this paper, the AWJT process of alumina ceramics is optimised for maximum MRR and minimum surface roughness. The MADEA, a variant of the DE algorithm, is used for optimisation. The MADEA algorithm is justified using 15 benchmark MOPs, from which the MADEA showed better performance in nine MOPs. The AWJT problem is also solved using six well-known MOEAs, NSGA-II, NSGA-III, MOEA/D, MOPSO, PESA2 and SPEA2. All the Pareto solutions obtained using evolutionary algorithms dominated the solution reported by the previous authors. One hundred forty-nine non-dominated solutions are calculated by MADEA, which is the maximum from any competing algorithm. The Pareto solutions of the algorithms are compared using seven performance metrics: IGD, spacing, coverage, CPF, ΔP, DM and PD. The performance metrics showed that MADEA was able to achieve better Pareto solutions than the considered true Pareto front. Also, MADEA produced the most diverse solutions, but the solutions were not uniformly spread.

Appendix

Table 3 Optimum solution provided by the comparison

Sr. no.	*Water pressure P [MPa]*	*Jet feed speed u [mm/s]*	*Abrasive mass flow rate ma [g/s]*	*Surface speed Vs [m/s]*	*Nozzle tilted angle β [°]*	*MRR, [μm³/μs]*	*Ra [μm]*
	x1	*x2*	*x3*	*x4*	*x5*		
1	310	0.25	11.5	6	71	5,441.96	3.41

Source: Yue et al. (2014a)

Table 4 Non-dominated solutions calculated using MADEA

Sr. no.	*Water pressure, P [MPa]*	*Jet feed speed u [mm/s]*	*Abrasive mass flow rate, ma [g/s]*	*Surface speed, Vs [m/s]*	*Nozzle tilted angle, β [°]*	*MRR, [μm³/μs]*	*R_a [μm]*
	x1	*x2*	*x3*	*x4*	*x5*		
1	190.307	0.050053	11.46976	4.981751	61.36492	4,038.805	2.806248
2	274.9199	0.050045	11.47695	5.990328	72.54915	6,083.87	3.597306
3	207.3339	0.050049	11.47394	5.702316	63.45485	4,482.622	2.97817
4	190.307	0.050053	11.46976	4.152742	61.36492	3,918.726	2.781906
5	303.6198	0.050032	11.48401	6.442994	79.10852	6,859.884	3.879002
6	205.3717	0.050048	11.47127	5.89032	61.10166	4,472.266	2.971728
7	309.5464	0.050031	11.48614	6.862138	95.60694	7,155.891	4.017634
8	303.6198	0.050032	11.48401	6.442994	80.05331	6,866.45	3.8813
9	280.7369	0.050038	11.48423	6.298434	79.07412	6,268.549	3.666391
10	209.6907	0.050048	11.46938	5.792861	62.55826	4,550.951	3.004478
11	212.4211	0.05005	11.4766	5.444959	60.83303	4,596.299	3.023897

Table 4 Non-dominated solutions calculated using MADEA (continued)

Sr. no.	Water pressure, P [MPa]	Jet feed speed u [mm/s]	Abrasive mass flow rate, ma [g/s]	Surface speed, Vs [m/s]	Nozzle tilted angle, β [°]	MRR, [μm³/μs]	R_a [μm]
	x1	x2	x3	x4	x5		
12	190.3069	0.050053	11.46839	4.065391	58.41859	3,936.243	2.786325
13	309.6896	0.050031	11.48006	6.460328	82.27998	7,039.383	3.943793
14	285.2248	0.050038	11.47859	6.072283	74.52687	6,350.066	3.695111
15	217.5603	0.050049	11.47436	5.746367	59.09326	4,750.947	3.085664
16	298.648	0.050036	11.48049	6.318988	79.0445	6,725.514	3.830914
17	221.0945	0.050042	11.4819	5.958702	66.13138	4,804.031	3.106309
18	302.8818	0.050031	11.48532	6.315844	82.12263	6,856.004	3.878264
19	298.648	0.050036	11.48049	6.318988	79.0445	6,725.514	3.830914
20	282.4839	0.050038	11.47962	6.246964	74.24314	6,291.734	3.673562
21	244.7876	0.050035	11.48203	5.888953	70.70921	5,344.458	3.318219
22	222.2271	0.050044	11.47429	5.891861	66.37125	4,823.386	3.114655
23	287.9966	0.050036	11.47401	6.396773	77.4114	6,448.373	3.731552
24	247.7548	0.050043	11.47597	5.766845	69.70624	5,407.501	3.342668
25	237.4123	0.050046	11.4753	5.977289	67.75514	5,181.498	3.254433
26	215.5711	0.050044	11.47622	5.898181	62.92813	4,691.742	3.060376
27	280.7369	0.050038	11.48423	6.298434	79.07412	6,268.549	3.666391
28	247.3033	0.050046	11.47467	5.792676	67.12557	5,403.506	3.340946
29	196.6751	0.050049	11.47436	5.886367	59.09326	4,295.211	2.898546
30	282.8091	0.050036	11.48476	6.235605	73.9248	6,299.409	3.675968
31	238.8204	0.050046	11.47467	5.792676	67.12557	5,203.187	3.263201
32	216.2376	0.050038	11.4742	5.977056	64.98409	4,698.357	3.064261
33	196.6751	0.050049	11.47436	5.886367	59.09326	4,295.211	2.898546
34	309.4075	0.050029	11.48598	7.041009	89.56743	7,107.473	3.981083
35	297.4909	0.050032	11.48312	5.940923	77.40225	6,663.947	3.809145
36	282.8428	0.050035	11.48497	6.255619	74.06802	6,301.934	3.676833
37	228.9837	0.050047	11.47465	5.855661	62.60012	4,997.775	3.182932
38	219.6907	0.05005	11.47026	5.798186	59.67633	4,798.5	3.104789
39	221.0945	0.050042	11.4819	5.958702	66.13138	4,804.031	3.106309
40	238.3032	0.050047	11.47877	5.968343	70.75873	5,192.391	3.260789
41	216.2698	0.050048	11.4707	5.833398	59.86521	4,723.29	3.073852
42	192.7156	0.050052	11.47443	5.771665	59.39783	4,194.643	2.857691
43	225.5083	0.050046	11.47127	5.871632	65.43629	4,903.593	3.14564
44	285.7295	0.050034	11.48136	6.248985	76.93319	6,383.787	3.706819
45	248.5522	0.050044	11.48265	6.229898	67.69568	5,462.984	3.363028
46	241.7645	0.050035	11.48416	5.834948	69.65716	5,270.582	3.289346

Table 4 Non-dominated solutions calculated using MADEA (continued)

Sr. no.	*Water pressure, P [MPa]*	*Jet feed speed u [mm/s]*	*Abrasive mass flow rate, ma [g/s]*	*Surface speed, Vs [m/s]*	*Nozzle tilted angle, β [°]*	*MRR, [μm³/μs]*	*R_a [μm]*
	x1	*x2*	*x3*	*x4*	*x5*		
47	196.6751	0.050049	11.47436	5.886367	59.09326	4,295.211	2.898546
48	291.9517	0.050033	11.48517	6.446139	78.32943	6,558.467	3.770426
49	246.8403	0.050041	11.47781	5.914057	68.57177	5,399.472	3.338486
50	309.8833	0.050129	11.49994	7.405179	104.6279	7,244.379	4.101012
51	190.0921	0.05003	11.49812	1.521212	63.25962	3,267.114	2.701869
52	190.0921	0.05003	11.49812	1.521212	63.25962	3,267.114	2.701869
53	309.8833	0.050129	11.49994	7.405179	104.6279	7,244.379	4.101012
54	245.3073	0.05007	11.49857	5.927892	70.25006	5,363.507	3.323944
55	212.2328	0.050088	11.49555	6.11712	60.76529	4,647.729	3.042335
56	261.5868	0.050023	11.49935	5.943992	74.44607	5,760.007	3.475289
57	227.446	0.05004	11.48644	5.954744	67.05044	4,948.818	3.163128
58	266.8946	0.050034	11.48983	6.052928	71.74418	5,893.821	3.524765
59	199.2377	0.050019	11.49247	5.684882	57.77453	4,350.729	2.920411
60	295.8972	0.050035	11.4941	6.139153	76.95964	6,637.483	3.797656
61	190.2116	0.050124	11.49317	4.632606	60.53881	3,999.692	2.797265
62	217.5531	0.050033	11.49389	6.09481	60.85268	4,766.726	3.089874
63	289.3623	0.050025	11.49748	6.187148	75.18729	6,468.318	3.736068
64	259.7679	0.050086	11.49971	6.24128	73.93239	5,732.968	3.46494
65	207.008	0.050036	11.48263	5.640204	58.50698	4,511.998	2.98765
66	264.582	0.050069	11.48812	5.880756	71.38739	5,824.323	3.499551
67	292.5259	0.050001	11.49574	6.114243	75.45759	6,544.036	3.763803
68	283.1517	0.050035	11.49998	6.233663	76.81388	6,322.659	3.682485
69	266.0818	0.050034	11.49692	5.884089	71.61136	5,863.712	3.513225
70	274.2432	0.050011	11.49684	5.97747	70.7177	6,067.558	3.590105
71	215.7256	0.05004	11.47971	5.84241	62.73373	4,692.896	3.060624
72	284.5466	0.05005	11.49522	6.157358	75.41042	6,346.403	3.691648
73	249.7838	0.050026	11.49029	5.787333	68.14936	5,463.255	3.36236
74	275.2379	0.050047	11.49612	6.132742	74.93345	6,111.54	3.605203
75	233.7303	0.05008	11.49093	5.997114	65.74667	5,105.836	3.223821
76	298.5245	0.050019	11.49549	6.185464	80.36141	6,728.006	3.830438
77	303.7112	0.050062	11.49696	6.447805	79.5881	6,869.584	3.880981
78	224.3836	0.050047	11.48634	5.599073	63.16401	4,869.612	3.132
79	229.8349	0.050048	11.49149	6.074549	64.55993	5,025.752	3.192252
80	243.3655	0.050013	11.4942	6.287056	69.13369	5,341.793	3.315349
81	293.1626	0.050005	11.49249	6.044791	77.35123	6,564.53	3.771342

Table 4 Non-dominated solutions calculated using MADEA (continued)

Sr. no.	Water pressure, P [MPa]	Jet feed speed u [mm/s]	Abrasive mass flow rate, ma [g/s]	Surface speed, Vs [m/s]	Nozzle tilted angle, β [°]	MRR, [μm³/μs]	R_a [μm]
	x1	x2	x3	x4	x5		
82	309.6733	0.05009	11.49832	6.33686	83.28289	7,046.514	3.944854
83	299.6485	0.050052	11.49862	6.376955	78.0901	6,753.328	3.839004
84	250.3091	0.050022	11.49909	6.199799	71.66508	5,500.563	3.376065
85	297.9166	0.050008	11.49643	6.231435	79.17244	6,708.196	3.822598
86	309.9541	0.050063	11.4919	6.92484	95.58111	7,169.974	4.021815
87	273.9887	0.050018	11.49944	6.377668	72.56603	6,089.628	3.597425
88	272.3914	0.050037	11.49886	6.267957	72.77042	6,044.898	3.580386
89	275.6194	0.050033	11.49077	6.323087	76.15188	6,133.559	3.614374
90	229.6528	0.050023	11.49162	6.168011	69.76277	5,002.845	3.186393
91	281.2197	0.05006	11.49937	6.131497	75.46257	6,262.912	3.660655
92	262.6645	0.050087	11.4945	6.17302	74.69252	5,799.93	3.49073
93	252.5344	0.050052	11.49046	6.245636	71.60921	5,555.362	3.39774
94	305.949	0.050044	11.49514	6.123828	79.22118	6,906.766	3.894326
95	308.8774	0.050116	11.49899	6.230635	81.85896	7,008.83	3.930816
96	285.2635	0.05002	11.49487	6.265149	74.52142	6,367.104	3.699497
97	190.0538	0.050011	11.49572	6.090926	59.11125	4,162.743	2.843605
98	262.8476	0.050013	11.49323	5.882871	70.90163	5,783.861	3.483413
99	280.1241	0.050048	11.49403	6.21788	75.35794	6,239.01	3.652362
100	216.2609	0.050025	11.48828	6.071404	63.9599	4,714.022	3.068952
101	302.9951	0.050055	11.48721	6.335481	80.14911	6,846.733	3.873799
102	290.2486	0.050085	11.4908	6.131157	76.66161	6,491.555	3.745344
103	282.7894	0.050048	11.48972	6.162869	74.76801	6,299.037	3.674949
104	288.5258	0.050037	11.49701	6.1359	75.21817	6,444.265	3.727363
105	196.733	0.050043	11.48508	5.645261	58.03411	4,288.425	2.895425
106	286.5652	0.05006	11.49793	6.204575	77.00765	6,406.99	3.713582
107	190.0538	0.050011	11.49572	3.550177	59.11125	3,828.387	2.765804
108	253.4203	0.050007	11.48345	6.218192	69.19072	5,576.927	3.40584
109	286.2494	0.050049	11.49915	6.099704	75.91343	6,388.613	3.706677
110	269.4622	0.050021	11.49126	5.917241	73.24238	5,949.876	3.545826
111	216.677	0.050033	11.48853	5.853325	60.41964	4,732.394	3.076101
112	190.0921	0.05003	11.49667	3.176132	62.51974	3,712.961	2.749419
113	265.1408	0.050076	11.49673	6.011606	70.56218	5,848.379	3.507719
114	271.6266	0.050065	11.49705	6.248452	74.18301	6,026.92	3.573937
115	267.1697	0.050025	11.49578	6.222756	73.11469	5,913.966	3.531653
116	282.5372	0.050027	11.49629	5.9391	75.04555	6,281.153	3.667972

Table 4 Non-dominated solutions calculated using MADEA (continued)

Sr. no.	*Water pressure, P [MPa]*	*Jet feed speed u [mm/s]*	*Abrasive mass flow rate, ma [g/s]*	*Surface speed, Vs [m/s]*	*Nozzle tilted angle, β [°]*	*MRR, [μm³/μs]*	*R_a [μm]*
	x1	*x2*	*x3*	*x4*	*x5*		
117	225.0095	0.050047	11.48716	5.911251	66.87758	4,889.083	3.139895
118	287.5981	0.050054	11.49446	6.191611	76.21573	6,427.907	3.721496
119	191.3225	0.050058	11.49795	3.327509	63.51081	3,762.846	2.764229
120	249.9034	0.050056	11.4951	6.056634	69.43286	5,484.159	3.3695
121	268.7549	0.050089	11.49592	5.898827	72.81505	5,930.779	3.538785
122	234.9769	0.050056	11.49977	6.03766	64.88835	5,142.828	3.237665
123	305.1295	0.050063	11.49949	6.324998	78.63405	6,894.066	3.889355
124	271.485	0.050047	11.49196	5.935417	72.84335	6,000.104	3.564575
125	200.4334	0.050013	11.49041	5.714879	57.20214	4,385.062	2.934602
126	199.2442	0.050014	11.49413	6.028463	58.32964	4,371.811	2.928962
127	256.7463	0.050068	11.49523	6.059624	71.18692	5,647.824	3.431908
128	225.0742	0.050066	11.49417	6.195082	67.89233	4,904.311	3.146725
129	209.5008	0.050061	11.47912	5.845912	60.37195	4,568.903	3.010504
130	217.4884	0.050041	11.49459	5.866029	60.55641	4,751.388	3.083458
131	241.9879	0.050085	11.49801	6.085964	69.97606	5,294.511	3.297538
132	243.4917	0.050088	11.49953	5.874958	67.91273	5,321.692	3.307289
133	277.4017	0.050126	11.47944	6.312292	73.31805	6,165.691	3.628024
134	233.5604	0.050034	11.48975	5.585928	64.97571	5,072.789	3.212168
135	290.6983	0.050013	11.4999	6.113591	79.18499	6,517.681	3.75415
136	221.9504	0.05002	11.48029	5.838908	65.09552	4,821.563	3.112498
137	276.6843	0.050059	11.49778	6.315222	73.08139	6,153.121	3.621024
138	190.0921	0.05003	11.49944	2.658637	62.51974	3,591.939	2.73453
139	202.9576	0.050018	11.47624	5.770798	59.54199	4,423.141	2.95082
140	210.8163	0.050043	11.48863	6.138085	62.88901	4,600.284	3.023601
141	228.7662	0.050042	11.48052	5.869402	64.77558	4,984.074	3.176476
142	190.5815	0.050064	11.49176	2.658847	61.57929	3,613.042	2.740164
143	209.8032	0.050062	11.49307	5.75784	58.22907	4,587.073	3.017991
144	308.749	0.050096	11.49707	7.138973	91.19325	7,106.061	3.98515
145	192.8689	0.05006	11.48735	6.059526	60.03794	4,212.876	2.865518
146	279.0401	0.050036	11.49667	6.254072	76.27984	6,217.627	3.644409
147	190.1277	0.05005	11.49144	5.201404	59.20922	4,085.091	2.817016
148	260.6473	0.050006	11.48648	5.629919	66.734	5,707.962	3.459138
149	190.4575	0.050009	11.49626	2.869859	61.22968	3,665.823	2.745239

References

Arun, A., Rajkumar, K. and Vishal, K. (2023) 'Process parameters for optimization in abrasive water jet machining (AWJM) of silicon-filled epoxy glass fibre polymer composites', *Journal of Inorganic and Organometallic Polymers and Materials*, 1 May, Vol. 33, No. 5, pp.1339–1356.

Balasubramaniyan, C., Manohar, N.J. and Esra, V. (2023) 'Abrasive water jet machining (AWJM) on glass fiber composite reinforced with aluminium waste grain: an experimental investigation', *Materials Today: Proceedings*, 22 August.

Coello, C.A.C. and Cortés, N.C. (2005) 'Solving multiobjective optimization problems using an artificial immune system', *Genetic Programming and Evolvable Machines*, Vol. 6, No. 1, pp.163–190.

Deb, K. and Jain, S. (2002) 'Running performance metrics for evolutionary multi-objective optimizations', *Proceedings of the Fourth Asia-Pacific Conference on Simulated Evolution and …*., pp.13–20.

Deb, K., Pratap, A., Agarwal, S. and Meyarivan, T. (2002) 'A fast and elitist multiobjective genetic algorithm: NSGA-II', *IEEE Transactions on Evolutionary Computation*, Vol. 6, No. 2, pp.182–197.

Ewees, A.A., Abd Elaziz, M. and Oliva, D. (2021) 'A new multi-objective optimization algorithm combined with opposition-based learning', *Expert Systems with Applications*, Vol. 165, No. 1, p.113844.

Flögel, K. and Faltin, F. (2013) 'Waterjet turning of titanium alloys', *Advanced Materials Research*, Vol. 769, No. 1, pp.77–84.

Ibrahim, S.A.B., Korkmaz, S., Cetin, M.H. and Kartal, F. (2020) 'Performance evaluation of the submerged abrasive water jet turning process for improving machinability of castamide', *Engineering Science and Technology, an International Journal*, Vol. 23, No. 4, pp.801–811.

Jain, N.K., Jain, V.K. and Deb, K. (2001) 'Optimization of process parameters of mechanical type advanced machining processes using genetic algorithms', *International Journal of Machine Tools and Manufacture*, Vol. 47, No. 6, pp.900–919.

Kartal, F. and Gökkaya, H. (2015) 'Effect of abrasive water jet turning process parameters on surface roughness and material removal rate of AISI 1050 steel', *Materials Testing*, Vol. 57, No. 9, pp.773–782.

Kartal, F. and Kaptan, A. (2023) 'Influence of abrasive water jet turning operating parameters on surface roughness of Abs and Pla 3d printed parts materials', *International Journal of 3D Printing Technologies and Digital Industry*, Vol. 7, No. 2, pp.184–190.

Kartal, F. and Yerlikaya, Z. (2016) 'Investigation of surface roughness and MRR for engineering polymers with the abrasive water jet turning process', *International Polymer Processing*, Vol. 31, No. 3, pp.336–345.

Kartal, F., Çetin, M.H., Gökkaya, H. and Yerlikaya, Z. (2014) 'Optimization of abrasive water jet turning parameters for machining of low density polyethylene material based on experimental design method', *International Polymer Processing*, Vol. 29, No. 4, pp.535–544.

Kartal, F., Yerlikaya, Z. and Gökkaya, H. (2017) 'Effects of machining parameters on surface roughness and macro surface characteristics when the machining of Al-6082 T6 alloy using AWJT', *Measurement*, Vol. 95, No. 1, pp.216–222.

Kasim, M.S. et al. (2022) 'Effect of abrasive water jet turning AWJT parameter setting on surface finish of Inconel 718', *International Journal of Nanoelectronics & Materials*, March, Vol. 15, Special issue, pp.271–279.

Liu, D., Huang, C.Z., Wang, J., Zhu, H.T., Yao, P. and Liu, Z.W. (2013) 'Study on the effect of standoff distance on processing performance of alumina ceramics in two modes of abrasive waterjet turning patterns', *Advanced Materials Research*, Vol. 797, No. 1, pp.21–26.

Rana, P. and Lalwani, D.I. (2017) 'Parameters optimization of surface grinding process using modified ε constrained differential evolution', *Materials Today: Proceedings*, Vol. 4, No. 9, pp.10104–10108.

Runarsson, T.P. et al. (2006) 'Problem definitions and evaluation criteria for the CEC 2006 special session on constrained real-parameter optimization', *Journal of Applied Mechanics*, Vol. 41, No. 8, pp.8–31.

Schott, J.R. (1995) 'Fault tolerant design using single and multicriteria genetic algorithm optimization', Air Force Inst. of Tech. Wright-Patterson afb OH1995.

Schutze, O., Esquivel, X., Lara, A. and Coello, C.A.C. (2012) 'Using the averaged Hausdorff distance as a performance measure in evolutionary multiobjective optimization', *IEEE Transactions on Evolutionary Computation*, Vol. 16, No. 4, pp.504–522.

Štefek, A., Raska, J., Hlavac, L.M. and Spadlo, S. (2021) 'Investigation of significant parameters during abrasive waterjet turning', *Materials (Basel)*, 5 August, Vol. 14, No. 16, p.4389.

Takahama, T. and Sakai, S. (2009) 'Efficient constrained optimization by the ε constrained differential evolution using an approximation model with low accuracy', *Transactions of the Japanese Society for Artificial Intelligence*, Vol. 24, No. 1, pp.34–45.

Tian, Y., Cheng, R., Zhang, X., Li, M. and Jin, Y. (2019) 'Diversity assessment of multi-objective evolutionary algorithms: Performance metric and benchmark problems [research frontier]', *IEEE Computational Intelligence Magazine*, Vol. 14, No. 3, pp.61–74.

Uhlmann, E., Flögel, K., Sammler, F., Rieck, I. and Dethlefs, A. (2014) 'Machining of hypereutectic aluminum silicon alloys', *Procedia CIRP*, vol. 14, pp.223–228.

Wang, H., Jin, Y. and Yao, X. (2017) 'Diversity assessment in many-objective optimization', *IEEE Transactions on Cybernetics*, Vol. 47, No. 6, pp.1510–1522.

Yue, Z., Huang, C., Zhu, H., Wang, J., Yao, P. and Liu, Z. (201a4) 'Optimization of machining parameters in the abrasive waterjet turning of alumina ceramic based on the response surface methodology', *The International Journal of Advanced Manufacturing Technology*, Vol. 71, Nos. 9–12, pp.2107–2114.

Yue, Z., Huang, C., Zhu, H., Yao, P. and Liu, Z. (2014b) 'Material removal analysis in the radial-mode abrasive waterjet turning of ceramic materials', *International Journal of Abrasive Technology*, Vol. 6, No. 4, pp.298–313.

Yue, Z.B., Huang, C.Z., Zhu, H.T., Wang, J., Yao, P. and Liu, Z.W. (2013) 'An experimental study on radial-mode abrasive waterjet turning of alumina ceramics', *Advanced Materials Research*, Vol. 797, No. 1, pp.27–32.

Zhang, X., Tian, Y., Cheng, R. and Jin, Y. (2015) 'An efficient approach to nondominated sorting for evolutionary multiobjective optimization,' *IEEE Transactions on Evolutionary Computation*, Vol. 19, No. 2, pp.201–213.

Zitzler, E. and Thiele, L. (1999) 'Multiobjective evolutionary algorithms: a comparative case study and the strength Pareto approach', *IEEE transactions on Evolutionary Computation*, Vol. 3, No. 4, pp.257–271.

Zohourkari, I., Zohoor, M. and Annoni, M. (2015) 'Investigation of the effects of machining parameters on material removal rate in abrasive waterjet turning', *Advances in Mechanical Engineering*, Vol. 6, No. 1, p.624203.

Nomenclature

MRR	Material removal rate	P_W	Water pressure
R_a	Surface roughness	β	Nozzle tilted angle
d	Depth of cut	SOD	Stand-off-distance
F	Feed	d_N	Nozzle diameter
n	speed		
d_p	particle size		
m_A	abrasive flow rate		